Resonant $L_{II,III}$ x-ray Raman scattering from HCl

C. Såthe,[1] F. F. Guimarães,[2,3] J.-E. Rubensson,[1] J. Nordgren,[1] A. Agui,[4] J. Guo,[5] U. Ekström,[6] P. Norman,[6] F. Gel'mukhanov,[2] and H. Ågren[2]

[1]*Department of Physics, Uppsala University, Box 530, S-751 21 Uppsala, Sweden*

[2]*Theoretical Chemistry, Roslagstullsbacken 15, Royal Institute of Technology, S-106 91 Stockholm, Sweden*

[3]*Departamento de Química, Universidade Federal de Minas Gerais, Avenue Antonio Carlos, 6627, CEP-31270-901, Belo Horizonte, MG, Brazil*

[4]*Synchrotron Radiation Research Unit, Japan Atomic Energy Agency, 1-1-1 Kouto, Sayo-cho, Sayogun, Hyogo 679-5148, Japan*

[5]*Advanced Light Source, Lawrence Berkeley National Laboratory, MS 6R2100, One Cyclotron Road, Berkeley, California 94720, USA*

[6]*Department of Physics, Chemistry and Biology, Linköping University, SE-581 83 Linköping, Sweden*

(Received 18 August 2006; published 27 December 2006)

We have studied the spectral features of Cl $L_{II,III}$ resonant x-ray Raman scattering of HCl molecules in gas phase both experimentally and theoretically. The theory, formulated in the intermediate-coupling scheme, takes into account the spin-orbital and molecular-field splittings in the Cl $2p$ shells, as well as the Coulomb interaction of the core hole with unoccupied molecular orbitals. Experiment and theory display nondispersive dissociative peaks formed by decay transitions in both molecular and dissociative regions. The molecular and atomic peaks collapse in a single narrow resonance because the dissociative potentials of core-excited and final states are parallel to each other along the whole pathway of the nuclear wave packet.

DOI: 10.1103/PhysRevA.74.062512 PACS number(s): 33.90.+h, 31.15.Ne, 32.30.Rj, 32.80.Hd

I. INTRODUCTION

The creation and decay of excited states are fundamental to all physical processes involving energy transfer on a microscopic scale. High-resolution resonant x-ray Raman scattering (RXS) of free molecules provides an excellent tool for investigating the finer details of the electronic structure, which reflects different aspects of the intramolecular interaction. In the case of resonant excitations below the ionization threshold, utilization of RXS opens up new prospects [1–5]. One of the main advantages of RXS is the possibility to study the same final state but making use of different intermediate core-excited states. Such an opportunity makes the interpretation of the molecular spectrum more accurate from the point of view of both occupied and virtual molecular orbitals (MO's).

The object of our combined experimental and theoretical study is the Cl $L_{II,III}$ RXS spectrum of the HCl molecule. This molecule was widely used in explorations of different dynamical effects accompanying x-ray excitation using the resonant Auger effect in the soft x-ray region [1,2] and RXS near the Cl K edge [6,7]. One of the major difficulties is that the core hole is in the $2p$ orbital of the chlorine atom, which is affected by substantial spin-orbit (SO) splitting. This splitting, about 1.75 eV, can be comparable with the Coulomb interaction between core and valence MO's involved in the scattering. This forces us to invoke the intermediate-coupling scheme [8] and to solve the corresponding equations explicitly. From our simulations of the x-ray absorption (XAS) and RXS spectra we are able to perform the theoretical assignment of the spectral lines, based on *ab initio* self-consistent field (SCF) and multiconfigurational SCF (MCSCF) calculations of the inner-shell excited states. Special attention is paid to the RXS through the dissociative core-excited state.

The article is organized as follows. We begin with a brief outline of the experiment in Sec. II. Section III includes the diagonalization of the molecular Hamiltonian with the chlorine L-shell spin-orbit interaction included followed by a derivation of the expression for the RXS cross sections of randomly oriented molecules. Details of the numerical simulations are described in Sec. IV. Analysis of simulations and comparison to the experiment are included in Sec. V. Our findings are summarized in Sec. VI.

II. EXPERIMENT

The experiments were carried out at beamline 7.0 at the Advanced Light Source at Lawrence Berkeley Laboratories [9]. The gas was contained in a sealed gas cell connected to a manifold where we could refresh the gas sample and keep a constant gas pressure. The pressure was monitored using Pirani tubes and kept at between 1 and 10 mbar depending on the excitation energy in order to avoid saturation and maximize intensity in the RXS measurements. The windows used were 1000-Å-thick Si_4N_3 entrance windows and 1500 -Å-thick polyimide film on a supporting mesh [10] as a window in the detection direction of RXS. The XAS was measured using a electrode measuring the current generated from the secondary electrons from the excitation process with a Kiethley picoamperemeter. The RXS was measured using a grazing incidence spherical grating spectrometer [11] mounted perpendicular to the incoming light and parallel to the polarization vector of the synchrotron radiation light. The slits on the monochromator were opened to get enough flux for the experiments. The grating used was a 5-m-radius spherical grating with 400 lines/mm with the slit set to 20 μm. The estimated spectral resolution is 500 meV in the x-ray emission spectra.

III. SOLUTION OF EIGENVALUE PROBLEM FOR CORE-EXCITED STATE

We start from diagonalization of the nonrelativistic many-electron molecular Hamiltonian H for the core-excited state

$|2p_c \rightarrow \bar{\psi}_\nu\rangle$ with $c=x,y,z$ and the vacant MO $\bar{\psi}_\nu$, where $\psi_\nu = \psi_\nu(\mathbf{r})\alpha$ and $\bar{\psi}_\nu = \psi_\nu(\mathbf{r})\beta$ are the spin-orbital functions with spin up (α) and spin down (β). The diagonalization of H gives the following eigenvalues and eigenfunctions for the singlet,

$$E_{c\nu}(S), \quad \Psi_{c\nu}(S) = \frac{1}{\sqrt{2}}(|\psi_c\bar{\psi}_\nu\rangle + |\psi_\nu\bar{\psi}_c\rangle), \quad c=x,y,z, \quad (1)$$

and the triplet,

$$E_{c\nu}(T), \quad \Psi^m_{c\nu}(T) = \begin{cases} |\psi_c\psi_\nu\rangle, & m=1 \\ |\bar{\psi}_c\bar{\psi}_\nu\rangle, & m=-1 \\ \frac{1}{\sqrt{2}}(|\psi_c\bar{\psi}_\nu\rangle - |\psi_\nu\bar{\psi}_c\rangle), & m=0, \end{cases} \quad (2)$$

states. We choose the molecular bond along the z axis. Due to the axial symmetry, $E_{x\nu}(q)=E_{y\nu}(q)$. The next step [8] is to take into account the SO interaction in the L shell of chlorine:

$$\mathcal{H} = H + V_{\mathrm{SO}}, \quad V_{\mathrm{SO}} = A(r)\mathbf{L}\cdot\mathbf{S}, \quad A(r) = \frac{1}{2c^2 r}\frac{\partial V}{\partial r}, \quad (3)$$

where $\mathbf{L}$ and $\mathbf{S}$ are the orbital and spin momentum operators of the $2p$ shell of Cl, V is the potential of interaction of the $2p$ electron with the molecule, and c is the speed of light; we use atomic units unless otherwise stated. The SO splitting

$$\Delta_{\mathrm{SO}} = E(2p_{1/2}^{-1}) - E(2p_{3/2}^{-1}) = \frac{3}{2}\zeta, \quad \zeta = \int_0^\infty R_{2p}^2 A(r) r^2 dr, \quad (4)$$

is treated here semiempirically. We used the experimental value $\Delta_{\mathrm{SO}}=1.75$ eV, which is in good agreement with our four-component calculations ($\Delta_{\mathrm{SO}}=1.62$ eV). The SO interaction mixes singlet (1) and triplet (2) states,

$$E_\Lambda: |\Phi_\Lambda\rangle = \sum_{c=x,y,z}\left[C_c^{(\Lambda)}(S)|\Psi_c(S)\rangle + \sum_{m=1,0,-1} C_{cm}^{(\Lambda)}(T) \times |\Psi_{cm}(T)\rangle\right], \quad (5)$$

where $\Lambda=1,\ldots,12$. The coefficients are solutions of the equations

$$[E_c(S) - E_\Lambda]C_c^{(\Lambda)}(S) + \sum_{c_1=x,y,z}\sum_{m=1,0,-1}\langle\Psi_c(S)|V_{\mathrm{SO}}|\Psi_{c_1 m}(T)\rangle C_{c_1 m}^{(\Lambda)}(T) = 0,$$

$$[E_c(T) - E_\Lambda]C_{cm}^{(\Lambda)}(T) + \sum_{c_1=x,y,z}[\langle\Psi_{cm}(T)|V_{\mathrm{SO}}|\Psi_{c_1}(S)\rangle C_{c_1}^{(\Lambda)}(S) + \sum_{m_1=1,0,-1}\langle\Psi_{cm}(T)|V_{\mathrm{SO}}|\Psi_{c_1 m_1}(T)\rangle C_{c_1 m_1}^{(\Lambda)}(T)] = 0. \quad (6)$$

The Hermitian SO operator has the following nonzero matrix elements:

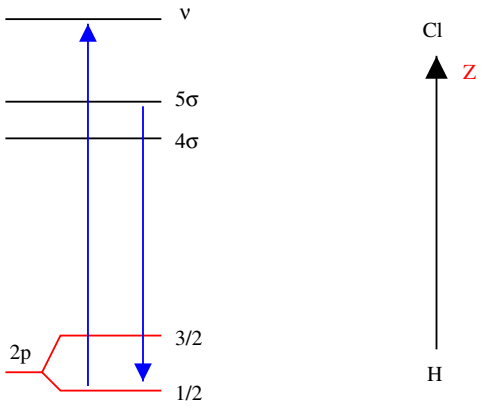

FIG. 1. (Color online) Scheme of the studied transitions.

$$\langle\Psi_c(S)|V_{\mathrm{SO}}|\Psi_{c_1,0}(T)\rangle = \frac{\iota}{2}\zeta\begin{cases}1, & c=y, \quad c_1=x, \\ -1, & c=x, \quad c_1=y,\end{cases}$$

$$\langle\Psi_c(S)|V_{\mathrm{SO}}|\Psi_{c_1,1}(T)\rangle = \langle\Psi_c(S)|V_{\mathrm{SO}}|\Psi_{c_1,-1}(T)\rangle^* = -\langle\Psi_{c,0}(T)|V_{\mathrm{SO}}|\Psi_{c_1,1}(T)\rangle = \langle\Psi_{c,0}(T)|V_{\mathrm{SO}}|\Psi_{c_1,-1}(T)\rangle^* = \frac{1}{2\sqrt{2}}\zeta\begin{cases}-\iota, & c=y, \quad c_1=z, \\ \iota, & c=z, \quad c_1=y, \\ -1, & c=x, \quad c_1=z, \\ 1, & c=z, \quad c_1=x,\end{cases}$$

$$\langle\Psi_{c,m}(T)|V_{\mathrm{SO}}|\Psi_{c_1,m}(T)\rangle = \frac{\iota}{2}m\zeta\begin{cases}1, & c=y, \quad c_1=x, \\ -1, & c=x, \quad c_1=y.\end{cases} \quad (7)$$

The solution of the coupled equations (1) and (2) produce eight different eigenvalues with four doubly degenerated levels, due to the symmetry of the molecule.

A. Inelastic x-ray Raman scattering

The amplitude of the resonant inelastic x-ray Raman scattering (RIXS) is given by the Kramers-Heisenberg formula (KH)

$$F_f(q) = \sum_{\Lambda=1}^{12}\frac{\langle 0|(\mathbf{e}\cdot\mathbf{D})|\Phi_\Lambda\rangle\langle\Phi_\Lambda|(\mathbf{e}_1\cdot\mathbf{D})|\Psi_f(q)\rangle}{\omega_1 - \omega_{\Lambda,f(q)} + \iota\Gamma}, \quad q=S,T, \quad (8)$$

where Γ is the lifetime broadening of the core-excited state; ω, $\mathbf{e}$ and ω_1, $\mathbf{e}_1$ are the frequencies and polarization vectors of the incident and scattered x-ray photons, respectively; $\omega_{\Lambda,f(q)}=E_\Lambda - E_f(q)$ is the resonant frequency of emission transition from the core-excited to the final singlet $[\Psi_f(q) = \Psi_f(S)]$ or triplet $[\Psi_f(q)=\Psi_f^m(T)]$ states. The core-excited state depends on the unoccupied molecular orbital ψ_ν (Fig. 1). The index ν of this MO is skipped for brevity of notation. It will be restored in Sec. III C to show the importance of the

interference of the elastic scattering channels through different unoccupied MO's. The transition dipole moments of core excitation $\langle 0|\mathbf{D}|\Psi_c(S)\rangle \approx \sqrt{2}\mathbf{d}_{c\nu}$ are expressed through the one-electron transition dipole moments between $2p_c$ and relaxed unoccupied MO ψ_ν. The matrix elements $\langle \Psi_c(q)|\mathbf{D}|\Psi_f(q)\rangle \approx \mathbf{d}_{cf}$ of the decay transitions $\psi_f \to 2p_c$ are approximated by the one-electron transition dipole moments, between the occupied MO ψ_f and the $2p$ core hole. The SO interaction in the core-excited state mixes singlet and triplet states (5). Due to this, in addition to the $S \to S \to S$ scattering channels the triplet channel, $S \to T \to T$, become accessible. The RXS amplitude of these channels reads

$$F_f(S) = \sqrt{2}\sum_{\Lambda=1}^{12} \frac{[\mathbf{e}\cdot\mathbf{D}^{(\Lambda)}(S)][\mathbf{e}_1\cdot\mathbf{D}_f^{(\Lambda)*}(S)]}{\omega_1 - \omega_{\Lambda,f(S)} + \imath\Gamma},$$

$$F_f^m(T) = \sqrt{2}\sum_{\Lambda=1}^{12} \frac{[\mathbf{e}\cdot\mathbf{D}^{(\Lambda)}(S)][\mathbf{e}_1\cdot\mathbf{D}_{fm}^{(\Lambda)*}(T)]}{\omega_1 - \omega_{\Lambda,f(T)} + \imath\Gamma}. \quad (9)$$

Here,

$$\mathbf{D}^{(\Lambda)}(S) = \sum_{c=x,y,z} C_c^{(\Lambda)}(S)\mathbf{d}_{c\nu},$$

$$\mathbf{D}_f^{(\Lambda)}(S) = \sum_{c=x,y,z} C_c^{(\Lambda)}(S)\mathbf{d}_{cf}, \quad \mathbf{D}_{fm}^{(\Lambda)}(T) = \sum_{c=x,y,z} C_{cm}^{(\Lambda)}(T)\mathbf{d}_{cf}. \quad (10)$$

The RXS cross section includes the scattering to singlet and triplet final states,

$$\sigma(\omega,\omega_1) = \sum_f \left[|F_f(S)|^2 \Phi(\omega_1 - \omega + \omega_{f(S),0}, \gamma) + \sum_{m=1,0,-1} |F_f^m(T)|^2 \Phi(\omega_1 - \omega + \omega_{f(T),0}, \gamma) \right], \quad (11)$$

where $\omega_{f(q),0} = E_f(q) - E_0$ is the frequency of the transition from ground to final singlet or triplet state. The spectral function of incident radiation is assumed to be a Gaussian

$$\Phi(\omega_1 - \omega + \omega_{f(q),0}, \gamma) = \frac{1}{\gamma}\sqrt{\frac{\ln 2}{\pi}} \exp\left[-\left(\frac{\omega_1 - \omega + \omega_{f(q),0}}{\gamma} \right)^2 \ln 2 \right], \quad (12)$$

with γ the half width at half maximum.

Let us tune an excitation energy ω far below the absorption edge:

$$\sqrt{\Omega^2 + \Gamma^2} \gg \Delta_{SO}, \Delta_{ST}, \quad \Omega = \omega - \omega_{edge}. \quad (13)$$

Here, Δ_{ST} is the singlet-triplet splitting of the core-excited state. The partial scattering amplitudes (9) show for such detuning collapse the multiplet structure in a single $S \to S \to S$ line:

$$F_f(S) \approx \frac{\sqrt{2}}{\Omega + \imath\Gamma} \sum_{c=x,y,z} (\mathbf{e}\cdot\mathbf{d}_{\nu c})(\mathbf{d}_{cf}\cdot\mathbf{e}_1),$$

$$F_f^m(T) \approx 0. \quad (14)$$

One can see complete quenching of the $S \to T \to T$ channel and the absence of SO splitting. This effect is rather similar to the collapse of vibrational structure studied earlier [1,7,12,13].

B. Orientational averaging

The present experiment deals with gas-phase molecules and fixed angle χ between $\mathbf{e}$ and the wave vector of the emitted photon, $\mathbf{k}_1$. The RXS cross section averaged over all molecular orientations is given by the same Eq. (11) with the partial contributions replaced by the averaged ones:

$$\overline{|F_f(S)|^2} = \frac{2}{9}\sum_{\Lambda=1}^{12}\sum_{\Lambda_1=1}^{12} \frac{1}{(\omega_1 - \omega_{\Lambda,f(S)} + \imath\Gamma)(\omega_1 - \omega_{\Lambda_1,f(S)} - \imath\Gamma)} \times \Bigg[\{\mathbf{D}^{(\Lambda)}(S)\cdot\mathbf{D}^{(\Lambda_1)*}(S)\}\{\mathbf{D}_f^{(\Lambda)*}(S)\cdot\mathbf{D}_f^{(\Lambda_1)}(S)\} + \frac{3}{20}(1 - 3\cos^2\chi) \times \Big(\{\mathbf{D}^{(\Lambda)}(S)\cdot\mathbf{D}_f^{(\Lambda)*}(S)\} \times \{\mathbf{D}^{(\Lambda_1)*}(S)\cdot\mathbf{D}_f^{(\Lambda_1)}(S)\} + \{\mathbf{D}^{(\Lambda)}(S)\cdot\mathbf{D}_f^{(\Lambda_1)}(S)\} \times \{\mathbf{D}^{(\Lambda_1)*}(S)\cdot\mathbf{D}_f^{(\Lambda)*}(S)\} - \frac{2}{3}\{\mathbf{D}^{(\Lambda)}(S)\cdot\mathbf{D}^{(\Lambda_1)*}(S)\} \times \{\mathbf{D}_f^{(\Lambda)*}(S)\cdot\mathbf{D}_f^{(\Lambda_1)}(S)\} \Big) \Bigg], \quad (15)$$

$$\overline{|F_f^m(T)|^2} = \frac{2}{9}\sum_{\Lambda=1}^{12}\sum_{\Lambda_1=1}^{12} \frac{1}{(\omega_1 - \omega_{\Lambda,f(T)} + \imath\Gamma)(\omega_1 - \omega_{\Lambda_1,f(T)} - \imath\Gamma)} \times \Bigg[\{\mathbf{D}^{(\Lambda)}(S)\cdot\mathbf{D}^{(\Lambda_1)*}(S)\}\{\mathbf{D}_{fm}^{(\Lambda)*}(T)\cdot\mathbf{D}_{fm}^{(\Lambda_1)}(T)\} + \frac{3}{20}(1 - 3\cos^2\chi) \times \Big(\{\mathbf{D}^{(\Lambda)}(S)\cdot\mathbf{D}_{fm}^{(\Lambda)*}(T)\} \times \{\mathbf{D}^{(\Lambda_1)*}(S)\cdot\mathbf{D}_{fm}^{(\Lambda_1)}(T)\} + \{\mathbf{D}^{(\Lambda)}(S)\cdot\mathbf{D}_{fm}^{(\Lambda_1)}(T)\} \times \{\mathbf{D}^{(\Lambda_1)*}(S)\cdot\mathbf{D}_{fm}^{(\Lambda)*}(T)\} - \frac{2}{3}\{\mathbf{D}^{(\Lambda)}(S)\cdot\mathbf{D}^{(\Lambda_1)*}(S)\} \times \{\mathbf{D}_{fm}^{(\Lambda)*}(T)\cdot\mathbf{D}_{fm}^{(\Lambda_1)}(T)\} \Big) \Bigg]. \quad (16)$$

Here, we introduced the scalar product of the complex vectors a and b without conventional complex conjugation of the bra vector $\mathbf{a}$: $\{\mathbf{a}\cdot\mathbf{b}\} = \Sigma_{k=x,y,z} a_k b_k$.

C. Elastic x-ray Raman scattering

Elastic scattering (REXS) differs qualitatively from inelastic RXS because the final state coincides with the ground state of the molecule. Due to this, only the $S \to S \to S$ channel is allowed. Another important point is that the unoccupied MO's, to which the core electron is promoted, are now the intermediate ones in the scattering process $2p \to \psi_\nu \to 2p$.

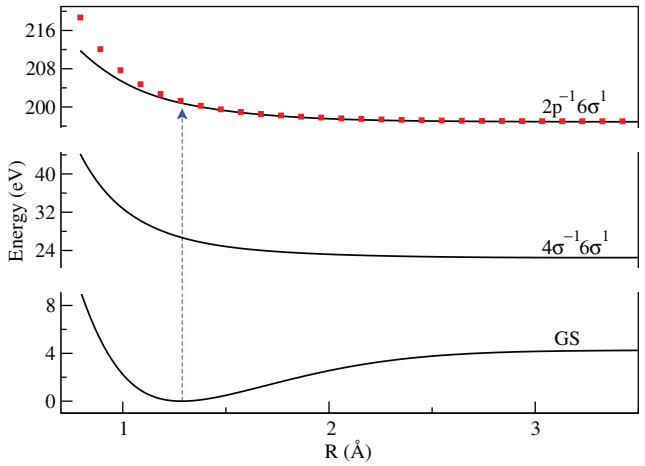

FIG. 2. (Color online) Potential surface of the ground (GS), first core-excited [18] $2p^{-1}6\sigma^1$, and final $4\sigma^{-1}6\sigma^1$ states. The squares display the final $4\sigma^{-1}6\sigma^1$ state potential shifted in energy to show the parallelism of the potentials.

This means that the scattering amplitude (9) for elastic scattering includes the sum over ν [1,14,15]:

$$F = \sqrt{2}\sum_{\nu}\sum_{\Lambda=1}^{12}\frac{[\mathbf{e}\cdot\mathbf{D}^{(\Lambda\nu)}(S)][\mathbf{e}_1\cdot\mathbf{D}^{(\Lambda\nu)*}(S)]}{\omega_1-\omega_{\Lambda\nu,0}+\imath\Gamma}. \tag{17}$$

Contrary to the inelastic scattering, the peak position of the cross section of the elastic channel coincides with the excitation energy:

$$\sigma(\omega,\omega_1) = |F|^2\Phi(\omega_1-\omega,\gamma). \tag{18}$$

Here we display the index of unoccupied MO's in $\mathbf{D}^{(\Lambda)}(S) \rightarrow \mathbf{D}^{(\Lambda\nu)}(S)$ and $\omega_{\Lambda 0}\rightarrow\omega_{\Lambda\nu,0}$ due to the importance of interference in the elastic scattering channels through different intermediate unoccupied MO's ψ_ν. The cross section of elastic scattering averaged over all molecular orientations is given by Eq. (18) with $|F|^2$ replaced by

$$\begin{aligned}\overline{|F|^2} = \frac{2}{9}\sum_{\nu}\sum_{\Lambda=1}^{12}\sum_{\nu_1}\sum_{\Lambda_1=1}^{12}&\frac{1}{(\omega_1-\omega_{\Lambda\nu,0}+\imath\Gamma)(\omega_1-\omega_{\Lambda_1\nu_1,0}-\imath\Gamma)}\\ &\times\Bigg[\{\mathbf{D}^{(\Lambda\nu)}(S)\cdot\mathbf{D}^{(\Lambda_1\nu_1)*}(S)\}\{\mathbf{D}^{(\Lambda\nu)*}(S)\cdot\mathbf{D}^{(\Lambda_1\nu_1)}(S)\}\\ &+\frac{3}{20}(1-3\cos^2\chi)\times\Big(\{\mathbf{D}^{(\Lambda\nu)}(S)\cdot\mathbf{D}^{(\Lambda\nu)*}(S)\}\\ &\times\{\mathbf{D}^{(\Lambda_1\nu_1)*}(S)\cdot\mathbf{D}^{(\Lambda_1\nu_1)}(S)\}+\{\mathbf{D}^{(\Lambda\nu)}(S)\cdot\mathbf{D}^{(\Lambda_1\nu_1)}(S)\}\\ &\times\{\mathbf{D}^{(\Lambda_1\nu_1)*}(S)\cdot\mathbf{D}^{(\Lambda\nu)*}(S)\}-\frac{2}{3}\{\mathbf{D}^{(\Lambda\nu)}(S)\cdot\mathbf{D}^{(\Lambda_1\nu_1)*}(S)\}\\ &\times\{\mathbf{D}^{(\Lambda\nu)*}(S)\cdot\mathbf{D}^{(\Lambda_1\nu_1)}(S)\}\Big)\Bigg].\end{aligned} \tag{19}$$

IV. COMPUTATIONAL DETAILS

The DALTON [16] molecular electronic structure package was used to compute the energies of the singlet and triplet core-excited and final states of HCl. We have applied the MCSCF level of calculation considering eight electrons in a complete active space (CAS) (6, 5, 5, 2) on the C_{2v} symmetry (A_1,B_1,B_2,A_2), where, for example, 6 means six orbitals of the A_1 symmetry. These calculations were performed with the core-correlated aug-cc-pCVTZ basis set [17]. Figure 2 shows the potential surfaces of the ground and core excited $2\pi^{-1}6\sigma^1$ states [18], as well as our result for the final state $4\sigma^{-1}6\sigma^1$. To take into account the SO interaction in the core-excited state we solved Eqs. (6) with $\Delta_{SO}=1.75$ eV. In order to get the SO splitting value we performed relativistic calculations based on the four-component STEX technique [19], as implemented in the DIRAC program [20]. For this calculation we decontracted the qaug-cc-pCVTZ [17] basis set and added tight p and d functions. The exponents for these tight functions were taken from a geometrical series of the two most tight p and d exponents in the original basis set. The RXS cross sections are computed for $\chi=0$, which correspond to the experimental value.

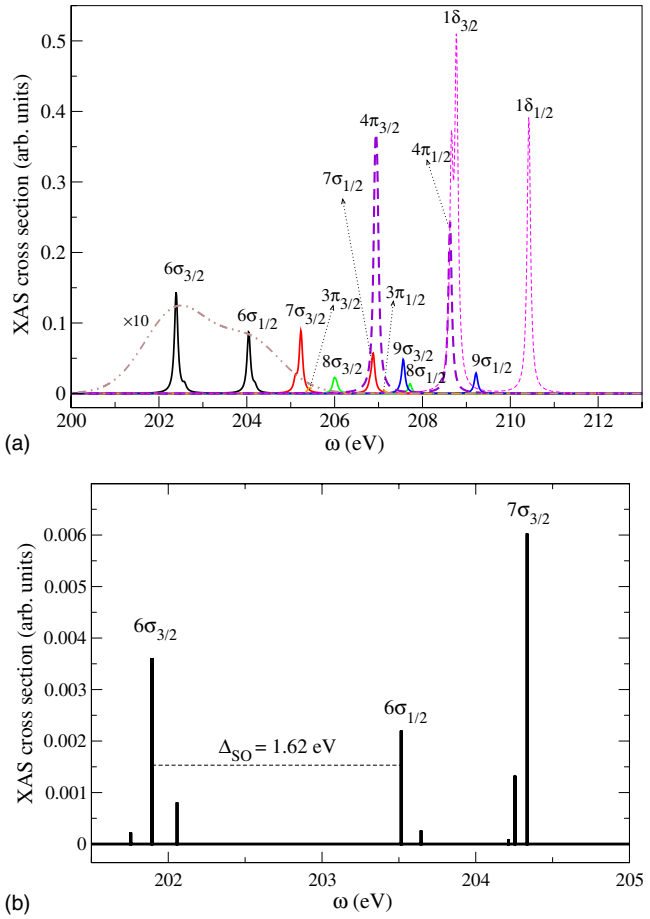

FIG. 3. (Color online) Theoretical Cl $L_{II,III}$ x-ray absorption spectrum of HCl. Solid lines in panel (a) show x-ray transitions to the σ levels, while the dashed lines show the XAS of π and δ subsystems shifted by −0.85 eV. $\Gamma=0.0465$ eV. Panel (b) shows the results of four-component simulations for the first three peaks in the Cl $L_{II,III}$ XAS spectrum of HCl.

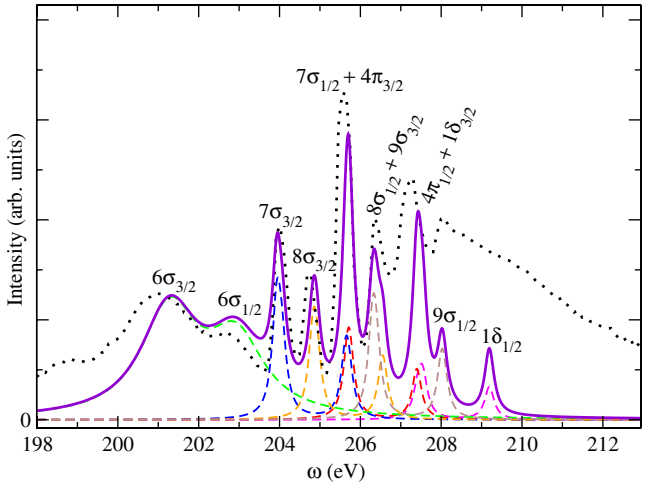

FIG. 4. (Color online) Comparison of the experimental $L_{II,III}$ XAS spectrum of the HCl spectrum (dotted line) with theoretical simulations (solid line) based on a rescaling of the transition dipole moment (see the text). The dashed lines show the partial contributions. $\Gamma=0.14$ eV for all states except dissociative $6\sigma_{3/2}$ and $6\sigma_{1/2}$ states with half width at half maximum equal to 0.84 eV.

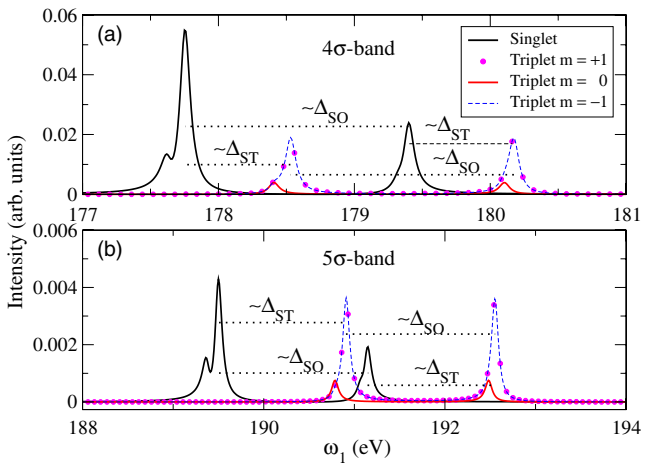

FIG. 5. (Color online) Partial contributions $|F_f(S)|^2$, Eq. (15), and $|F_f^m(T)|^2$, Eq. (16), for the core excitation of the 7σ level (Fig. 3). The inset shows the spin of the final state under scattering. Δ_{ST} is the singlet-triplet splitting of the final state.

V. DISCUSSION OF EXPERIMENTAL AND SIMULATED RESULTS

A. X-ray absorption

Our simulations of L x-ray absorption are based on the following expression for the absorption cross section averaged over all molecular orientations:

$$\sigma(\omega)=\frac{2}{3}\sum_{\nu}\sum_{\Lambda=1}^{12}|\mathbf{D}^{(\Lambda)}(S)|^2\Delta(\omega-\omega_{\Lambda 0},\Gamma),\quad \omega_{\Lambda 0}=E_\Lambda-E_0. \tag{20}$$

In the MCSCF simulations of XAS we take into account the following transitions: $2p\rightarrow 6\sigma,7\sigma,8\sigma,9\sigma$ and $2p\rightarrow 3\pi,4\pi,1\delta$ [Fig. 3(a)]. The relativistic calculations based on the four-component STEX technique [19] show rather similar intensities of the components of the first spin doublet, and it gives $\Delta_{SO}=1.62$ eV [Fig. 3(b)], which is close to the experimental spin-orbital splitting $\Delta_{SO}\approx 1.75$ eV. The underestimation of Δ_{SO} is due to the use of the Dirac-Coulomb Hamiltonian, which neglects spin-other-orbit effects. Both MCSCF and STEX calculations show the fine structure of each component of the spin doublet caused by the molecular-orbital splitting of the core shell, as well as by the Coulomb interaction between the $L_{II,III}$ shell and the vacant MO. We see mainly triplet and doublet fine structure of bands $6\sigma_{3/2}$ and $6\sigma_{1/2}$, respectively. We label the core-excited state $|2p_j^{-1}\nu^1\rangle$ as ν_j, with $j=1/2,\ 3/2$. The accuracy of our MCSCF simulations of σ and π subsystems is very sensitive to the CAS. To get better agreement with the experiment, we shifted the π and δ peaks to a lower-energy region by 0.85 eV [Fig. 3(a)]. A rather similar displacement of the π levels relative to the σ subsystem was observed earlier in XAS of the OCS molecule [21]. The first spin doublet related to core excitation to 6σ MO (marked in Fig. 3 as $6\sigma_{3/2}$ and $6\sigma_{1/2}$) is computed taking into account only lifetime broadening Γ. However, the transition to the 6σ MO is essentially broader because the first core-excited state is dissociative (Fig. 2). We simulated the dissociative broadening of the first spin doublet using the wave packet technique [18]. The results of the simulations are shown in Fig. 3(a) by the dot-dashed line. Figure 3(a) reproduces all experimental features in the XAS spectrum (Fig. 4) after the above-mentioned shift of the π and δ resonances. However, the intensity ratio obtained from the MCSCF calculation is far from being perfect. For instance, the 7σ intensity is severely underestimated compared to the experiment and also compared to the STEX calculation. The difference between the intermediate-coupling MCSCF and four-component STEX calculations is not mainly due to a different treatment of relativistic effects, but rather due to basis set differences and because of the way

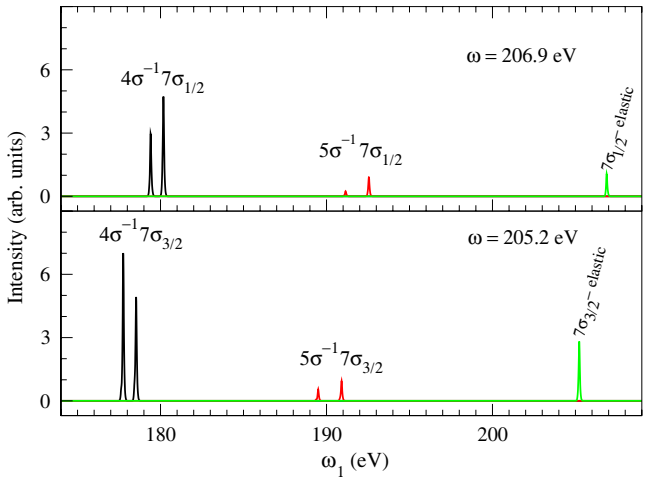

FIG. 6. (Color online) RXS spectra of HCl for different excitation energies. $\omega=206.9$ eV and $\omega=205.2$ eV correspond to excitation of the $7\sigma_{3/2}$ and $7\sigma_{1/2}$ states, respectively [Fig. 3(a)]. Incident x-ray photons with different excitation energies "cut off" different parts of the partial contributions (Fig. 5) according to Eq. (11).

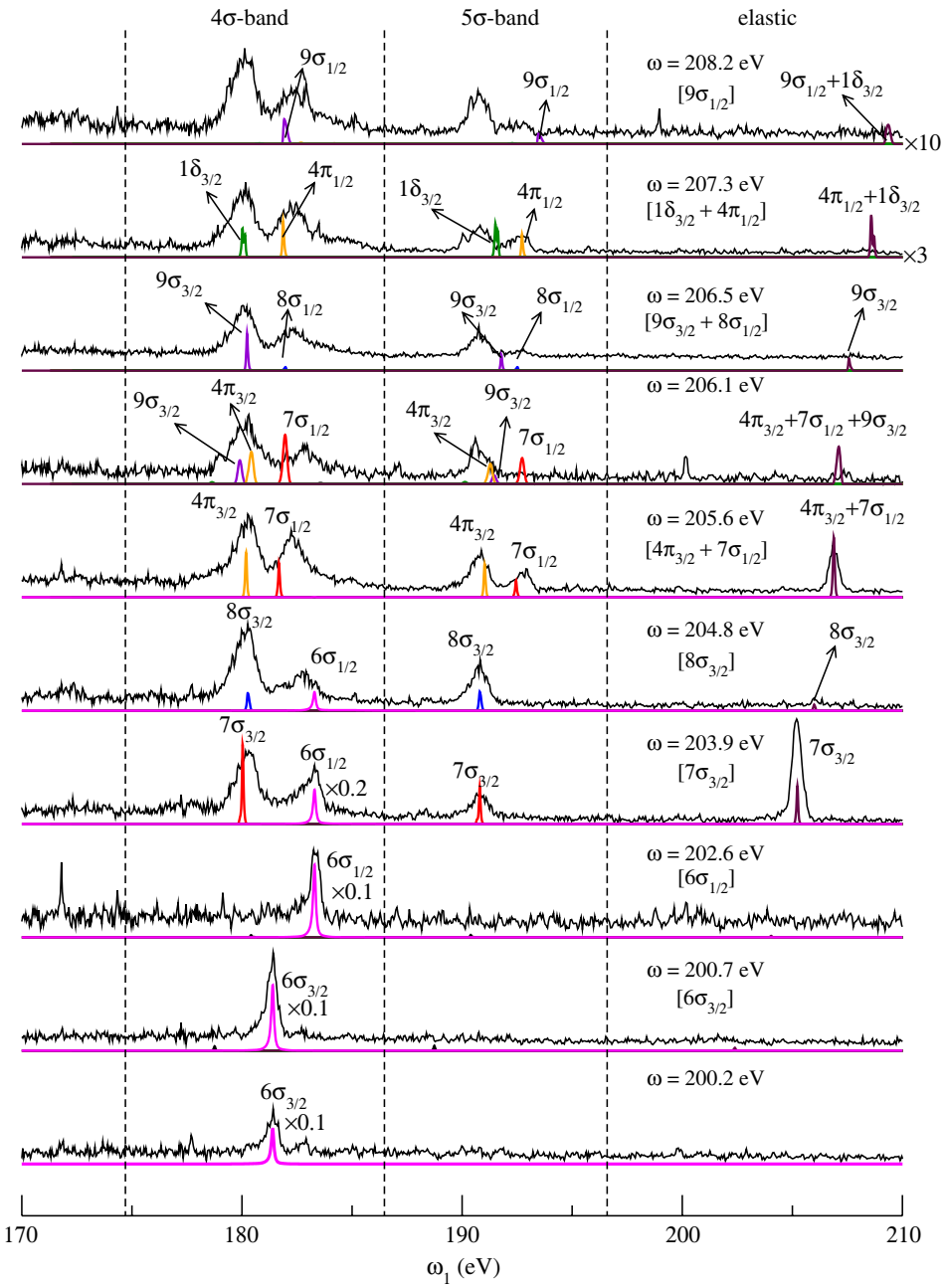

FIG. 7. (Color online) Experimental and theoretical RXS spectra of HCl for different excitation energies. The label below the excitation energy shows the corresponding resonant peak in the x-ray absorption, Fig. 4. The theoretical spectra were computed using the data from Fig. 4. The 4σ and 5σ bands obtained by MCSCF calculations were shifted to higher energy regions by 2.28 eV and 1.3 eV, respectively. The intensity of all theoretical elastic peaks is reduced by a factor of 5 times compared with inelastic resonances. Theoretical spectra in the two upper panels were increased by 10 and 3 times, respectively.

electron correlation is treated in the these two methods. Due to this, we rescaled the transition dipole moments by fitting our theoretical MCSCF profile to the experiment (Fig. 4). In this fitting we have modified all the transition dipole moments used in Eq. (6) and shifted the whole spectral profile, Fig. 3(a), to a lower-energy region by 1.25 eV.

B. X-ray Raman scattering

Let us start by illustrating the formation of the RXS profile upon excitation to 7σ MO. According to Eq. (11), the RXS profile is the product of the spectral function and of the partial contributions $|F_f(S)|^2$, Eq. (15), and $|F_f^m(T)|^2$, Eq. (16). Figure 5 displays the spectral shape of the partial contribution for final states containing holes in the 4σ and 5σ occupied MO's. These bands include sidebands related to transitions to the final singlet and triplet states. The scattering to the final triplet state is allowed due to the SO interaction in the core-excited state. Each of these sidebands is split due to the SO interaction and the molecular-field splitting of the core shell, as well as because of the Coulomb interaction of the core hole with the 7σ vacant level. The spectral function for different excitation energies "cut off" different parts of the partial contributions (Fig. 5) according to Eq. (11) (see Fig. 6). One can also see the elastic peak.

Both experimental and theoretical RXS spectral profiles for different excitation energies are shown in Fig. 7. The 4σ and 5σ bands obtained by MCSCF calculations were shifted to higher-energy regions by 2.28 eV and 1.3 eV, respectively.

The peaks $6\sigma_{3/2}$ and $6\sigma_{1/2}$ deserve a special comment. The origin of these resonances is the scattering through the

dissociative core-excited state $2p^{-1}6\sigma$ (see Fig. 2). Simulations show that the intensity of the band 5σ is much smaller than the intensity of the 4σ peak. Due to this, let us focus our attention only on an analysis of $4\sigma \rightarrow 2p$ fluorescence. The ground-state nuclear wave packet is promoted to the potential of the core-excited state and moves from the point of the vertical transition to the region of higher bond lengths (Fig. 2). During the dissociation in core-excited states, the molecules continuously decay to the final dissociative state $|2p^{-1}4\sigma\rangle$. A previous study of the resonant Auger spectra of HCl suggests that hydrogen has the time to approach the region of dissociation [22]. As is well known [1,18,23], the RXS profile in general consists of two qualitatively different bands. Decays near the equilibrium geometry form the molecular band while decay transitions in the dissociative region (where the potentials of the core-excited and final states are parallel) result in the so-called atomic peak. Contrary to the molecular band the peak position of the atomic peak does not depend on the excitation energy ω (except in the hard x-ray region [7]). However, the final- and core-excited-state potentials in the studied case are parallel to each other along the whole pathway of the wave packet (Fig. 2). This means that the molecular and atomic bands coincide with each other and they form a single nondispersive atomic peak, as one can see clearly from our wave packet simulations of the RSX channels $6\sigma_{3/2}$ and $6\sigma_{1/2}$. Nondispersive behavior of the corresponding experimental peaks confirms our simulations and interpretation (Fig. 2).

To conclude let us discuss shortly the elastic band. Figure 7 shows that the simulations give the relative intensity of the elastic peak approximately 5 times larger than the experiment. One of the reasons for this can be the self-absorption which is strong for resonant elastic scattering [1,15]. Another source of this disagreement with the experiment is the Thomson scattering [15,24] ignored in our simulations.

VI. SUMMARY

We were able to measure the Cl $L_{II,III}$ resonant x-ray Raman scattering spectra of HCl in a broad region of excitation energies. Both the experiment and theory, based on the intermediate-coupling scheme, show a strong dependence of the RXS profile on excitation energy. We observed that the excitation to the first dissociative core-excited state results in a narrow nondispersive resonance without any molecular band. The origin of this effect is that the dissociative potentials of the core-excited and final states are almost parallel to each other along the whole pathway of the nuclear wave packet. Our measurements and simulations show that the hydrogen has time to approach the region of dissociation due to the rather long lifetime of the core-excited state. This is in agreement with resonant Auger studies of the HCl molecule.

ACKNOWLEDGMENTS

This work was supported by the Swedish Research Council (VR) and Carl Tryggers Stiftelse (CTS) foundation.

[1] F. Gel'mukhanov and H. Ågren, Phys. Rep. **312**, 91 (1999).
[2] S. L. Sorensen and S. Svensson, J. Electron Spectrosc. Relat. Phenom. **114–116**, 1 (2001).
[3] K. Ueda, J. Phys. B **36**, R1 (2003).
[4] J. Nordgren and J. Guo, J. Electron Spectrosc. Relat. Phenom. **110–111**, 1 (2000).
[5] J.-E. Rubensson, J. Electron Spectrosc. Relat. Phenom. **110–111**, 135 (2001).
[6] S. H. Southworth, D. W. Lindle, R. Mayer, and P. L. Cowan, Phys. Rev. Lett. **67**, 1098 (1991).
[7] M. Simon, L. Journel, R. Guillemin, W. C. Stolte, I. Minkov, F. Gel'mukhanov, P. Sałek, H. Ågren, S. Carniato, R. Taïeb, A. C. Hudson, and D. W. Lindle, Phys. Rev. A **73**, 020706(R) (2006).
[8] N. A. Shkyaeva, L. N. Mazalov, and V. V. Murakhtanov, J. Struct. Chem. **20**, 621 (1979).
[9] T. Warwick, P. Heimann, D. Mossessain, W. MacKinney, and H. Padmore, Rev. Sci. Instrum. **66**, 2037 (1995).
[10] Custom-made window from Metorex International Oy, P.O. Box 85, FIN-02201 Espoo, Finland.
[11] J. Nordgren, G. Bray, S. Cramm, R. Nyholm, J-E. Rubensson, and N. Wassdahl, Rev. Sci. Instrum. **60**, 1690 (1989).
[12] F. Gel'mukhanov, T. Privalov, and H. Ågren, Phys. Rev. A **56**, 256 (1997).
[13] F. Hennies, S. Polyutov, I. Minkov, A. Pietzsch, M. Nagasono, F. Gel'mukhanov, L. Triguero, M.-N. Piancastelli, W. Wurth, H. Ågren, and A. Föhlisch, Phys. Rev. Lett. **95**, 163002 (2005).
[14] F. Gel'mukhanov and H. Ågren, Phys. Rev. A **50**, 1129 (1994).
[15] F. Gel'mukhanov and H. Ågren, Phys. Rev. A **56**, 2676 (1997).
[16] T. Helgaker, H. J. Aa. Jensen, P. Jørgensen, J. Olsen, K. Ruud, H. Ågren, A. A. Auer, K. L. Bak, V. Bakken, O. Christiansen, S. Coriani, P. Dahle, E. K. Dalskov, T. Enevoldsen, B. Fernandez, C. Hättig, K. Hald, A. Halkier, H. Heiberg, H. Hettema, D. Jonsson, S. Kirpekar, R. Kobayashi, H. Koch, K. V. Mikkelsen, P. Norman, M. J. Packer, T. B. Pedersen, T. A. Ruden, A. Sanchez, T. Saue, S. P. A. Sauer, B. Schimmelpfenning, K. O. Sylvester-Hvid, P. R. Taylor, and O. Vahtras. Dalton, a molecular electronic structure program, release 1.2, 2001. See http://www.kjemi.uio.no/software/dalton/dalton.html
[17] K. A. Peterson and T. H. Dunning, Jr. J. Chem. Phys. **117**, 10548 (2002).
[18] P. Sałek, F. Gel'mukhanov, and H. Ågren, Phys. Rev. A **59**, 1147 (1999).
[19] U. Ekström, P. Norman, and V. Carravetta, Phys. Rev. A **73**, 022501 (2006).
[20] H. J. Aa. Jensen, T. Saue, and L. Visscher, with contributions from V. Bakken, E. Eliav, T. Enevoldsen, T. Fleig, O. Fossgaard, T. Helgaker, J. Laerdahl, C. V. Larsen, P. Norman, J. Olsen, M. Pernpointner, J. K. Pedersen, K. Ruud, P. Salek, J.

N. P. van Stralen, J. Thyssen, O. Visser, and T. Winther. Dirac, a relativistic *ab initio* electronic structure program, release DIRAC04.0, 2004. see http://dirac.chem.sdu.dk

[21] V. Brems, B. M. Nestmann, and S. D. Peyerimhoff, Chem. Phys. Lett. **287**, 255 (1998).

[22] O. Björneholm, S. Sundin, S. Svensson, R. R. T. Marinho, A. Naves de Brito, F. Gel'mukhanov, and H. Ågren, Phys. Rev. Lett. **79**, 3150 (1997).

[23] P. Morin and I. Nenner, Phys. Rev. Lett. **56**, 1913 (1986).

[24] V. A. Yavna, A. N. Hopersky, A. M. Nadolinsky, and S. A. Yavna, J. Phys. B **33**, 3249 (2000).